Proton Direct Ionization Upsets at Tens of MeV

Andrea Coronetti, *Associate Member, IEEE*, Rubén García Alía, *Member, IEEE*, David Lucsanyi, Jialei Wang, *Graduate Student Member, IEEE*, Frédéric Saigné, Arto Javanainen, *Member, IEEE*, Paul Leroux, *Senior Member, IEEE*, and Jeffrey Prinzie, *Member, IEEE*

***Abstract*— Experimental monoenergetic proton single-event upset (SEU) cross sections of a 65-nm low core-voltage static random access memory (SRAM) were found to be exceptionally high not only at low energies (<3 MeV), but also at energies >3 MeV and extending up to tens of MeV. The SEU cross section from 20-MeV protons exceeds the 200-MeV proton SEU cross section by almost a factor of 3. Similarly, monoenergetic neutron cross sections at 14 MeV are about a factor of 3 lower than the 20-MeV proton cross section. Because of Monte Carlo (MC) simulations, it was determined that this strong enhancement is due to the proton direct ionization process as opposed to the elastic and inelastic scattering processes that dominate the SEU response above 3 MeV in other SRAMs. As shown by means of a detailed energy deposition scoring analysis, however, this does not appear to be caused by the critical charge of the SRAM being lower than the charge resulting from the average proton ionization through the linear energy transfer (LET). On the other hand, this is caused by high-energy δ-rays (>1 keV) that can deposit their full kinetic energy within the sensitive volume (SV) of a cell despite their range being theoretically much longer than the characteristic size of the SV. Multiple Coulomb scattering events are responsible for increasing the trajectory path of the δ-rays within the SV, resulting in a six-fold increase in the probability of upset with respect to the sole electron ionization.**

***Index Terms*— Delta-rays, Monte Carlo (MC) simulations, proton direct ionization, single-event upset (SEU).**

I. Introduction

DIRECT ionization from low-energy protons (LEPs) and related upsets in highly integrated memory devices have been a subject of study for one and a half decades [1], [2], [3], [4], [5], [6], [7], [8], [9], [10], [11], [12], [13], [14], [15], [16]. When the critical charge is low enough (as it is the case for advanced node technologies, <90 nm [5]), even LEPs can have sufficient linear energy transfer (LET) [0.1–0.5 MeV/(mg/cm^2)] to cause a bit flip [16].

Direct ionization upsets from protons can be observed as a result of monoenergetic experiments at energies below 3 MeV. Above this energy, the average LET of protons in silicon is further reduced well below 0.1 MeV/(mg/cm^2) [17], [18]. Consequently, the charge collected through direct ionization is not expected to exceed the critical charge. At the same time, other physical processes, such as elastic and inelastic scattering, can cause proton-induced upsets above 3 MeV [19], [20], [21]. In these cases, the major source of ionization is a secondary recoil ion with much higher LET than the primary proton [up to tens of MeV/(mg/cm^2)].

Secondary ions are produced as a result of the interaction between the proton and the nucleus of an atom. These processes are, however, characterized by low cross sections (i.e., only one in several thousand primary protons will experience a nuclear interaction in a nanometric volume). Oppositely, each primary proton will interact with the electronic cloud of one or several atoms of the semiconductor, mostly resulting in total ionizing dose (TID), but, sometimes, also in single-event upsets (SEUs).

The amount of kinetic energy that is transferred by the protons to these electrons, or δ-rays, can vary. Most of the electrons generated have very low kinetic content and will deposit all their energy near the proton trajectory, i.e., within the ionization track. However, if the energetic content is high enough, these δ-rays can travel much farther and further ionize other atoms (i.e., create additional electron–hole pairs) along their trajectory.

δ-rays carry part of the ionization potential of any ionizing particle passing through matter and are, therefore, very important for the accuracy of numerical tools used to simulate energy deposition in semiconductor devices, such as full transport Monte Carlo (MC) codes. Pure electron ionization can be considered of relevance for highly integrated technologies, because it was shown that upsets from a low-energy electron beam in static random access memories (SRAMs) are possible [22], [23]. In addition, the generation of high-energy δ-rays along the ionization structures of ions and LEPs can sensibly increase the number of upsets observed in these kinds of technologies [24], [25], [26]. In the last case, the δ-rays are so energetic that they can not only intersect several atoms, but even many separate sensitive volumes (SVs) along their trajectory.

In a previous work [16], monoenergetic proton SEU cross sections of three SRAMs sensitive to direct ionization from protons were measured. For one of these chips, the measured SEU cross section at energies ≥3 MeV did not decrease as

Manuscript received 26 August 2022; accepted 15 September 2022. Date of publication 20 September 2022; date of current version 18 April 2023. This work was supported in part by the European Union's Horizon 2020 Research and Innovation Program under MSC Grant 721624 and Grant 101008126, and in part by the European Space Agency [ESA/European Space Research and Technology Center (ESTEC)] at the University of Jyväskylä under Contract 4000124504/18/NL/KML/zk.

Andrea Coronetti is with CERN, 1211 Geneva, Switzerland, and also with the Institut d'Électronique et des Systèmes, Université de Montpellier, 34090 Montpellier, France (e-mail: andrea.coronetti@cern.ch).

Rubén García Alía and David Lucsanyi are with CERN, 1211 Geneva, Switzerland.

Jialei Wang, Paul Leroux, and Jeffrey Prinzie are with the Department of Electrical Engineering (ESAT), Katholieke Universiteit (KU) Leuven, 2440 Geel, Belgium.

Frédéric Saigné is with the Institut d'Électronique et des Systèmes, Université de Montpellier, 34090 Montpellier, France.

Arto Javanainen is with the Department of Physics, University of Jyväskylä, 40014 Jyväskylä, Finland, and also with the Electrical Engineering and Computer Science Department, Vanderbilt University, Nashville, TN 37235 USA.

Color versions of one or more figures in this article are available at https://doi.org/10.1109/TNS.2022.3207877.

Digital Object Identifier 10.1109/TNS.2022.3207877

sharply as it should based on the proton LET, but kept gradually decreasing up to tens of MeV. This behavior is different from that of the other two SRAMs or other data available in the literature. Even if it is generally noted that SEU cross sections of SRAMs of similar technology in the 20–50-MeV energy range are typically higher than at hundreds of MeV, this increase is typically limited to less than 50%, whereas for the particular SRAM under consideration, it reached almost a factor of 3.

This work is devoted to studying the reasons behind this abnormally high SEU cross section at energies above 3 MeV. This is investigated by means of detailed energy deposition scoring functionalities available from MC simulations. With these tools, one can calculate the contribution to the overall SEU cross section of each physical process at play. Later, these tools also help to determine the features of the high-energy δ-rays that dominate the SEU induction process for protons with primary energy in the order of tens of MeV.

II. Experimental Observations

The experimental data [16] were collected at various accelerators capable of delivering quasi-monoenergetic low- and high-energy protons [respectively, Centro Nacional de Aceleradores (CNA) [27] and Radiation Effect Facility (RADEF) [28], [29] for low- and intermediate-energy protons (<20 MeV), and PARTREC [30] and Paul Scherrer Institute (PSI) [31] for high-energy protons (>20 MeV)]. The experimental details are reported in [16] and [32]. Other than the proton cross sections, it is relevant to report the 14-MeV neutron cross sections [32], [33] (measured at Frascati Neutron Generator (FNG) [34]) in order to compare it with proton cross sections in the few tens of MeV energy interval.

The data under analysis are those of two SRAMs. One is a custom-built SRAM whose core voltage is tunable (0.3–1.2 V) [35], hereafter called the RADSAGA SRAM. All data reported refer to the minimum core voltage, i.e., 0.3 V. The other SRAM is a commercial memory from ISSI, hereafter called ISSI SRAM (with a core voltage of 0.85 V). The former SRAM shows enhanced proton SEU cross section, whereas the latter is taken for comparison purposes only, because it is considered as representative of the state of the art in terms of proton SEU response for low, intermediate, and high energy.

The experimental cross sections are reported in Figs. 1 and 2, for the ISSI and RADSAGA SRAMs, respectively. Only one device for each reference was tested. The data are plotted with error bars calculated at 95% confidence level considering a 10% error on the fluence provided by all the facilities and a $(2/\sqrt{N})$ error on the number of SEUs. Since each data point is the result of several thousands of SEUs, the error bar is dominated by the error on the fluence. However, being this very small and given the several orders of magnitude scale of the y-axis, the error bars in the plots may be smaller than the markers and not be always visible.

A comparison of the experimental cross sections of the two SRAMs highlights the different responses at the intermediate energies of (3–20 MeV) and even at high energies (>20 MeV). At 3 MeV, the SEU cross section of the RADSAGA SRAM is about two orders of magnitude lower if

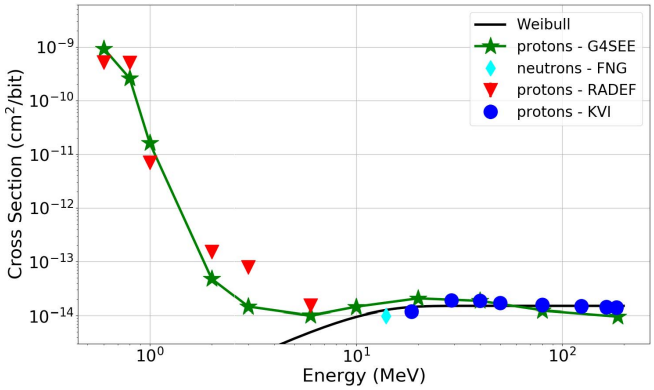

Fig. 1. Low-, intermediate-, and high-energy proton and 14-MeV neutron experimental SEU cross sections as a function of hadron energy for the ISSI SRAM. The high-energy proton data are fit with a Weibull with the following parameters: $\sigma_{sat} = 1.5 \times 10^{-14}$ cm^2/bit, $E_0 = 0$ MeV, $W = 10$ MeV, and $s = 1.8$. The data are compared with the G4SEE simulated cross sections.

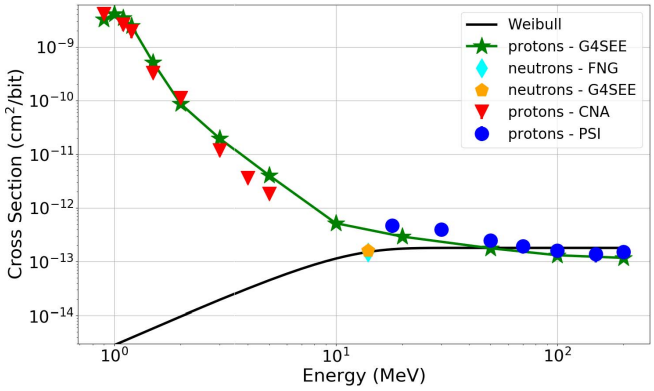

Fig. 2. Low-, intermediate-, and high-energy proton and 14-MeV neutron experimental SEU cross sections as a function of hadron energy for the RADSAGA SRAM when tuned at 0.3 V. The high-energy proton data are fit with a Weibull with the following parameters: $\sigma_{sat} = 1.8 \times 10^{-13}$ cm^2/bit, $E_0 = 0$ MeV, $W = 10$ MeV, and $s = 1.8$. The data are compared with the G4SEE simulated cross sections.

compared with the peak value at 0.9 MeV. On the other hand, the SEU cross section of the ISSI SRAM at this same energy is almost four orders of magnitude lower than the peak value at 0.6 MeV.

The experimental 14-MeV neutron cross section of the ISSI SRAM well aligns with the proton data at 6 and 18 MeV. A factor of ≈3 difference exists when comparing the experimental 14-MeV neutron to the 18-MeV proton cross section for the RADSAGA SRAM.

If the proton cross sections of both SRAMs were fully dominated by elastic and inelastic scattering processes at energies between 10 and 20 MeV, they would be expected to either match those of neutrons of similar energy (for which direct ionization is not possible) or to be slightly lower due to the additional Coulomb repulsion between the proton and the nucleus of the atom. However, the fact that the experimental SEU cross section is approximately three times higher is a first valuable indication that direct ionization from protons may be important at few tens of MeVs for the RADSAGA SRAM.

III. Proton SEU Cross Sections by Physical Process

The Geant4-based [36] G4SEE tool [37] is used to perform MC simulations of energy deposition in the SVs of these

two SRAMs. The SV models are the same obtained with FLUKA [16], [38] and [39]. In summary, the ISSI model is a cubic rectangular parallelepiped (RPP) of side 310 nm and a critical charge of 0.96 fC (corresponding $E_{\text{crit}} = 21.6$ keV), whereas the RADSAGA RPP model has a square surface with a side of 640 nm, a thickness of 250 nm, and a critical charge of 0.55 fC (corresponding $E_{\text{crit}} = 12.4$ keV).

Finally, the two models have different back-end-of-line (BEOL; 6 versus 12 μm of SiO_2, a simplification of the actual BEOL), though at the energies under consideration (5–20 MeV), this is not expected to have any significant impact on the results, because the energy lost by the protons is <3% with respect to the energy prior to the BEOL (e.g., a proton with an energy of 5 MeV prior to the BEOL will reduce its energy down to 4.91 MeV after the BEOL of the ISSI and down to 4.82 MeV for the BEOL of the RADSAGA SRAM).

The use of G4SEE enabled access to several features useful for this work.

1) A better fit of the ISSI experimental cross section at intermediate energy is achieved through G4SEE without any change to the RPP model described in [16]. The strong underestimation from FLUKA was due to the approximative treatment of the nuclear elastic scattering process in FLUKA (threshold at 10 MeV).
2) The possibility to enable/disable physical processes in G4SEE allowed extracting SEU cross sections of these SV models on a process-by-process basis for both protons and δ-rays.
3) The detailed energy deposition scoring tool allows obtaining a deeper insight into the nature of the particles (type and energy) behind the energy deposition events that contribute to the SEU triggering.

G4SEE numerical SEU cross sections for the two SRAMs are reported in Figs. 1 and 2, and they include all relevant mechanisms. The fitting achieved with the experimental data is very good at any proton energy.

The main physical processes behind proton upsets in SRAMs are through electromagnetic (direct ionization and Coulomb elastic scattering) and nuclear processes (nuclear elastic and inelastic scattering, which also includes complex nuclear reactions).

By running various simulations with only one of these processes enabled, the contribution of each physical process to the proton SEU cross section can be disentangled. This results in plots, such as those in Figs. 3 and 4 for the two SRAMs, respectively.

Concerning the processes themselves, there a few noteworthy features. The Coulomb elastic scattering process, while being present at any proton energy, does not contribute in a very significant fashion to the overall proton SEU cross section at any primary proton energy. Only for the ISSI SRAM, it is just a minor contributor for the 3-MeV data point.

The nuclear elastic scattering becomes significant (or even the most important) only above 3 MeV and up to few tens of MeV. Below this energy range, it is much lower than direct ionization and, above, than nuclear inelastic scattering.

The nuclear inelastic scattering becomes dominant at ≈20 MeV, and it is less significant at lower energies. All these

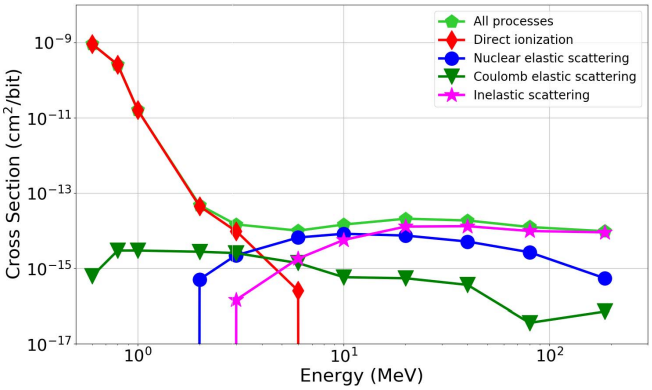

Fig. 3. Low-, intermediate-, and high-energy proton SEU cross sections as a function of the primary proton energy for the ISSI SRAM by physical process. Results retrieved with G4SEE.

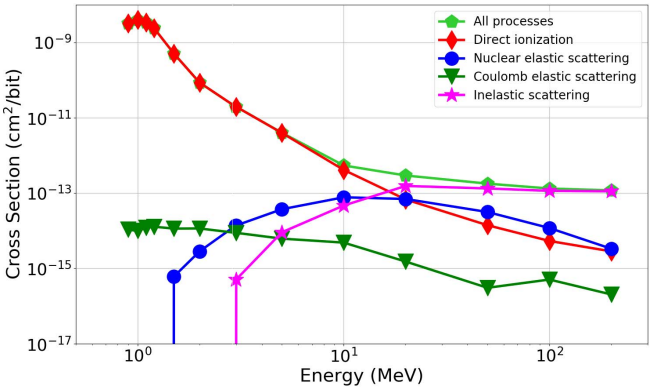

Fig. 4. Low-, intermediate-, and high-energy proton SEU cross sections as a function of the primary proton energy for the RADSAGA SRAM when tuned at 0.3 V by the physical process. Results retrieved with G4SEE.

three processes share similar trends among the two SRAM models.

On the other hand, the contribution to the proton SEU cross section of direct ionization differs between the two SRAM models straight after the peak (which is reached at different energies due to the diverse BEOL). As generally expected, the contribution from direct ionization for the ISSI SRAM completely disappears above 3 MeV. On the other hand, the contribution for the RADSAGA SRAM remains dominant up to 10 MeV, and it is still an important contributor at 20 MeV and at least as relevant as the nuclear elastic scattering at any higher primary proton energy.

This is a somewhat unexpected result, but it is, to the best of our knowledge, the only way to justify such a high experimental SEU cross section in the 3–20-MeV energy range. Nevertheless, given the small LET of the protons of these energies, the average proton ionization does not seem to provide enough justification for these findings. Therefore, a detailed scoring analysis is used to investigate where these high amounts of energetic events, exceeding the critical charge, are originating from.

Before moving deeper within the physics behind these SEUs, it may be important to perform a checkup about the accuracy of these simulation results. For nanometric volumes and MC simulations, the generation and explicit transport of δ-rays within the medium can have very important

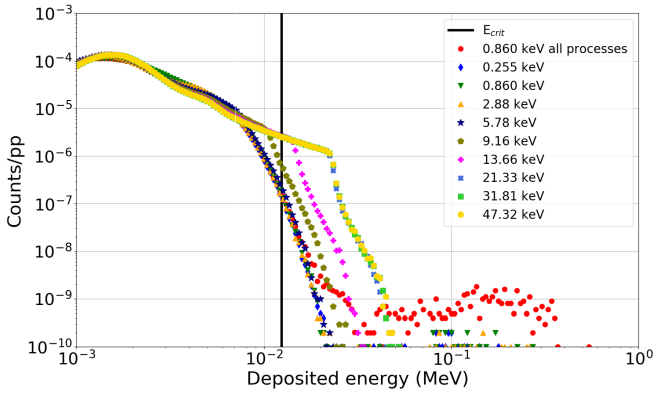

Fig. 5. Effect of changing the energy threshold for production of δ-rays in G4SEE on the energy deposition spectrum for the RADSAGA SRAM SV model with only the proton direct ionization process enabled. A case with all processes enabled is also reported to show that the events from the other processes become important only at around twice the critical energy of the SRAM. The primary particles are 10-MeV protons.

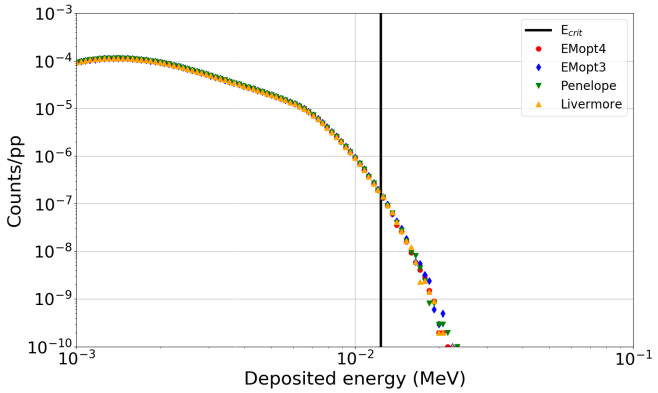

Fig. 6. Effect of changing the electromagnetic physics library in Geant4 on the energy deposition spectrum for the RADSAGA SRAM SV model with only the proton direct ionization process enabled. The primary particles are 10-MeV protons.

consequences on the results. This is defined by means of a production threshold in terms of either energy or range of the δ-rays. This means that all δ-rays below this production threshold are not explicitly generated and transported. Their energy is fully deposited locally at the point of the primary proton ionization track where they would have been generated. As a result, their full kinetic energy is deposited. On the contrary, if the δ-ray has an energy exceeding the production threshold, it is generated and transported through the various media until its energy becomes null. Using a production threshold in MC simulations is required to keep the simulation time reasonable.

Simulation results are affected, because if this threshold is set too high, then δ-rays that could have escaped the nanometric SV will not be generated and will, hence, deposit in the SV their full kinetic energy.

Fig. 5 depicts the spectra of energy deposited in the RADSAGA SRAM SV, as the δ-ray energy threshold is changed for a 10-MeV primary proton beam. The energy threshold used in the previous plots was 0.860 keV. Other values in the 0.255–47.32-keV energy threshold range have been simulated while keeping only the proton direct ionization process enabled. What the plot shows is that for the SV under consideration, there is basically no difference in the number of energy deposition events exceeding the critical energy if the production threshold is lower than $\sim$5 keV. This means that no information is lost if δ-rays below this energy are not explicitly generated and transported, because they are anyway expected to deposit their full energy in an SV of this size.

On the other hand, at higher production thresholds, the amount of events exceeding the critical energy rapidly increases by orders of magnitude. This increase stops at $\sim$22 keV, which is the theoretical upper limit for the energy that a 10-MeV proton can transfer to a δ-ray, according to [40]

$$E_{\max} = \frac{2m_e c^2(\gamma^2 - 1)}{1 + 2\gamma \frac{m_e}{M} + \left(\frac{m_e}{M}\right)^2} \tag{1}$$

where m_e = electron mass, M = proton mass, c = speed of light, and γ = Lorentz factor.

This shows that if δ-ray production thresholds above 5 keV are employed, an overestimation in the simulated SEU cross section would appear.

The choice of the Geant4 physics library may also affect the numerical results due to the different transport models employed for the δ-rays. Concerning the data reported in this work, the transport of the δ-rays in G4SEE was handled through the ElectroMagnetic Physics Option4 (EMopt4) library.

Simulations with another three physics modules implementing different δ-ray transport models (EMopt3, Penelope, and Livermore) were performed. A comparison among the energy deposition distributions resulting from the implementation of these libraries is available in Fig. 6 for the 10-MeV proton primary energy with only hadron ionization enabled. The distributions look quite similar, and the tiny differences at the higher energies yield a maximum discrepancy among the numerical SEU cross sections of just $\pm 2\%$ with respect to EMopt4.

Therefore, it can be concluded that the selection of the physics library would actually have little impact on the transport of δ-rays, which is relevant for the following analysis.

IV. Detailed Scoring of Proton Direct Ionization

The detailed scoring functionality of G4SEE allows scoring the characteristics of the primary and secondary particles depositing energy while passing through the SV of the device. Only δ-rays having an energy above 0.860 keV are scored, because this is the energy threshold set for production and which is low enough according to Fig. 5.

In the following energy deposition histograms, these distributions are considered.

1) *Proton p^+ Energy Deposition:* Caused by protons passing through the SV and based on the energy deposition due to low-energy δ-rays ($E < 0.860$ keV), typically, the peak of this distribution is located around the tabulated LET for the primary proton energy.
2) δ_{in} *Energy Deposition:* Caused by one or a few δ-rays with energy above 0.860 keV that are generated by a proton passing inside the SV.
3) δ_{out} *Energy Deposition:* Caused by one or a few δ-rays with energy above 0.860 keV that are generated by a

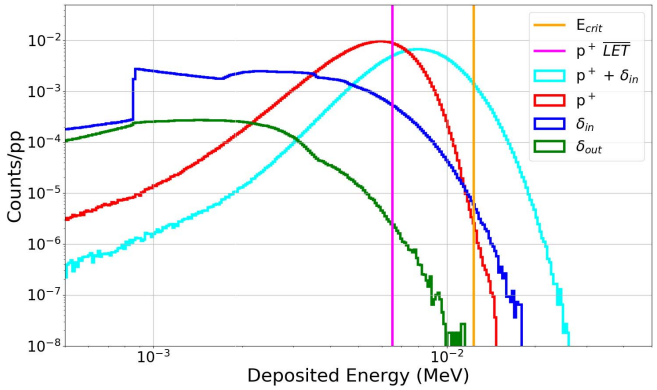

Fig. 7. Energy deposition histogram for the RADSAGA SRAM from a primary proton energy of 2 MeV. The data are separated to distinguish energy deposition caused by protons (p^+), high-energy δ-rays generated inside (δ_{in}) and outside (δ_{out}) the SV, and by the combination of proton and δ-rays ($p^+ + \delta_{\text{in}}$) inside the SV.

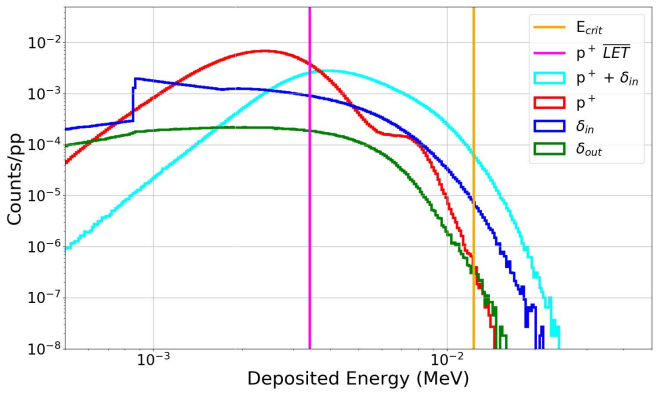

Fig. 8. Energy deposition histogram for the RADSAGA SRAM from a primary proton energy of 5 MeV. The data are separated to distinguish energy deposition caused by protons (p^+), high-energy δ-rays generated inside (δ_{in}) and outside (δ_{out}) the SV, and by the combination of proton and δ-rays ($p^+ + \delta_{\text{in}}$) inside the SV.

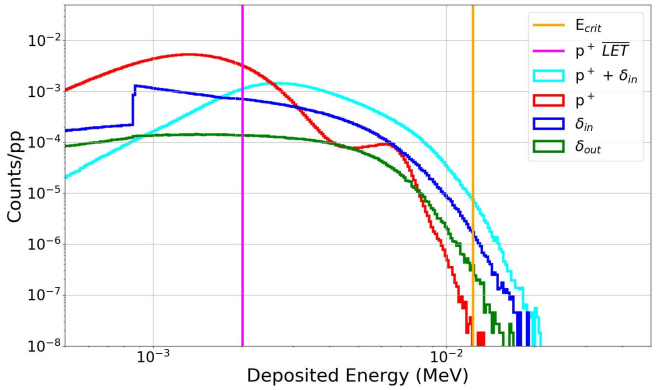

Fig. 9. Energy deposition histogram for the RADSAGA SRAM from a primary proton energy of 10 MeV. The data are separated to distinguish energy deposition caused by protons (p^+), high-energy δ-rays generated inside (δ_{in}) and outside (δ_{out}) the SV, and by the combination of proton and δ-rays ($p^+ + \delta_{\text{in}}$) inside the SV.

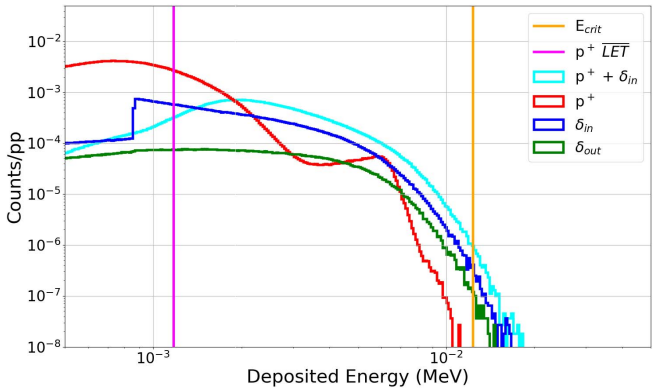

Fig. 10. Energy deposition histogram for the RADSAGA SRAM from a primary proton energy of 20 MeV. The data are separated to distinguish energy deposition caused by protons (p^+), high-energy δ-rays generated inside (δ_{in}) and outside (δ_{out}) the SV, and by the combination of proton and δ-rays ($p^+ + \delta_{\text{in}}$) inside the SV.

proton passing outside the SV and that travel inside the SV.

It is noted that all δ_{in} events are accompanied by the presence of a proton inside the SV. Therefore, the cumulative energy deposition of such an event is given by the summation of the energy deposited by the proton through low-energy δ-rays around the ionization track and that of these high-energy δ-rays that proceeds further away from the proton ionization track. For this reason, in the histograms, also, the $p^+ + \delta_{\text{in}}$ energy deposition distributions are shown.

Finally, the plots also mark a couple of noteworthy energy levels. The first one (p^+ $\overline{\text{LET}}$) is the energy that, on average, a proton of a given energy is expected to deposit in silicon over a length equal to the thickness of the SV. The second one (E_{crit}) is the critical energy (analog to the critical charge) of the SRAM.

Figs. 7–10 show the histograms of energy deposition from direct ionization for protons having a primary energy of 2, 5, 10 and 20 MeV, respectively.

As the plots show, when the energy increases, a decreasing amount of p^+-type energy depositions can lead to an SEU. At 20 MeV, p^+-type events not accompanied by the generation of high-energy δ-rays are indeed not expected to generate any SEU.

On the other hand, high-energy δ-rays generated inside the SV yield an energy deposition that, alone, would be sufficient to cause upsets at any of the considered primary proton energies. Actually, since the energy transferred to the high-energy δ-rays increases with the primary proton energy, starting at 5 MeV, even high-energy δ-rays generated outside the SV can yield events energetic enough to trigger an SEU.

Regarding the $p^+ + \delta_{\text{in}}$ energy deposition distributions, a shape transition is observed, as the energy increases. In the region around the E_{crit}, the shape of this distribution resembles that of protons at 2-MeV primary proton energy. However, at higher energy, the shape tends to resemble more and more that of the high-energy δ-rays generated inside the SV, with proton energy deposition through low-energy δ-rays becoming less and less significant.

This is further highlighted in Fig. 11, where, for each primary proton energy, the contribution of δ_{in} to the energy deposition in $p^+ + \delta_{\text{in}}$ events in the cases in which the critical energy of the SRAM is exceeded is shown. As depicted in the plot, at 2 MeV, the distribution is centered around 0.5, meaning that 50% of the energy deposition is coming from

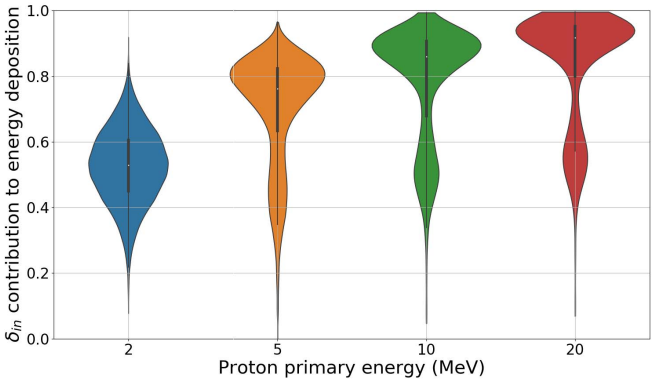

Fig. 11. Probability distributions for the energy deposition contribution of δ_{in} in $p^+ + \delta_{\text{in}}$ events exceeding the critical energy for different primary proton energies. The width of a bin is normalized to the number of events in that bin.

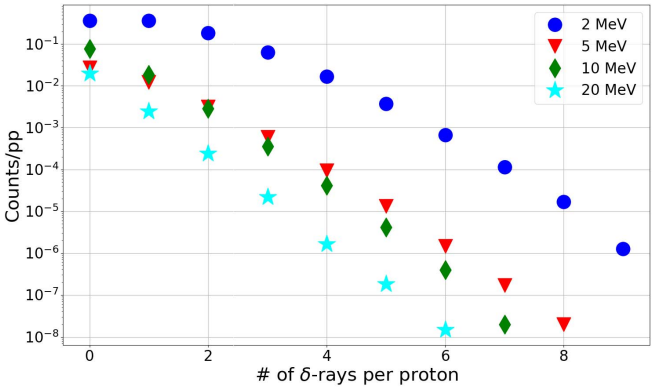

Fig. 12. Amount of δ-rays per primary proton that exceed the production threshold of 0.860 keV from the primary proton energies of 2–20 MeV. Data apply to the RADSAGA SRAM SV.

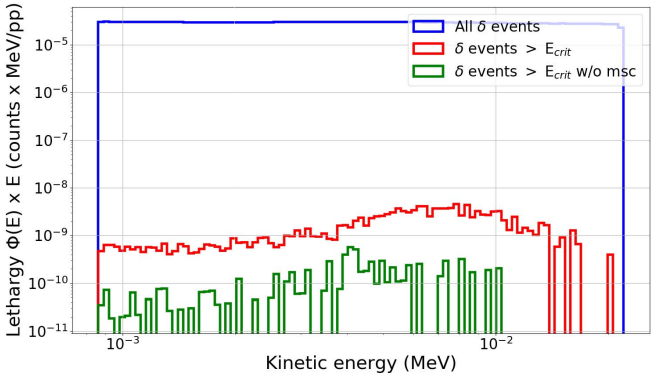

Fig. 13. Lethargy of δ-rays from primary protons with an energy of 10 MeV. The blue curve considers all δ-rays. The red curve only those yielding events overpassing the critical energy of the SRAM. The green curve is the same as the red, but in this case, Coulomb scattering events for δ-rays are disabled.

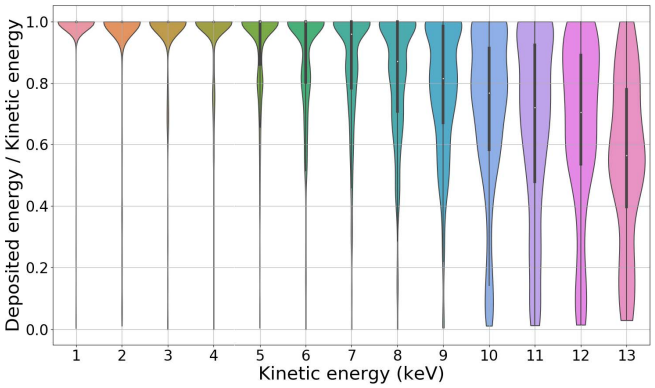

Fig. 14. Fraction of δ-ray kinetic energy that is deposited inside the SV as a function of the δ-ray kinetic energy for those δ-rays that lead to events exceeding the critical energy of the SRAM. δ-rays from 10-MeV protons. The width of a bin is normalized to the number of events in that bin.

low-energy δ-rays (<0.860 keV) and the other 50% from high-energy δ-rays (>0.860 keV).

At higher primary proton energies, it becomes increasingly likely that the high-energy δ-rays in events exceeding the critical charge contribute to 70%–90% to the total energy deposition. It is noted that the δ-ray contributions may have a hard cutoff at the top, lower than 1, because there will always be a minimal amount of energy deposited by the primary proton.

In summary, the generation of high-energy long-range δ-rays (both inside and outside the SV) and the related energy deposition events can explain the observed experimental SEU cross sections for the 3–20 MeV range when it comes to direct ionization effects.

V. Nature and Mechanism of δ-Ray Upsets in Proton Direct Ionization

The δ-ray events depicted in the previous plots are a result of the production of one or more δ-rays by a single proton interacting with the silicon atoms. G4SEE also allows determining the contribution to the total energy deposition down to the individual δ-rays in these events. This allows, for instance, to retrieve the kinetic energy and the energy deposited by each of these particles.

Fig. 12 depicts the amount of δ-rays per primary proton that are produced by protons with the primary energies of 2–20 MeV in the RADSAGA SRAM SV. The multiplicity of δ-rays per primary proton decreases exponentially regardless of the primary proton energy.

Taking 10 MeV as a reference, ~80% of the total proton fluence will not yield any δ-ray with an energy above production threshold (0.860 keV). The probability of producing a single δ-ray is lower than 20%, whereas producing two or more δ-rays comes with a cumulative probability of <3% no matter the primary proton energy.

The figure also shows that when the primary proton energy increases, the probability of producing several δ-rays dramatically decreases by orders of magnitude.

Concerning the 10 MeV case, Fig. 13 presents the lethargy of the δ-rays as a function of their kinetic energy. The plot shows that there is equal probability for δ-rays to be generated with any kinetic energy between the production threshold and the maximum kinetic energy that a proton can transfer to them. The figure also reports about the kinetic energy of the δ-rays that belong to events that overpass the critical energy of the SRAM. Despite the lower statistics, it is clear that δ-rays with energies up to around 13 keV can contribute to events that can overpass the critical energy. On the other hand, higher energy δ-rays would typically keep escaping from the SV.

It is noted that single high-energy δ-rays that can deposit enough energy to exceed the critical energy (12.4 keV) are

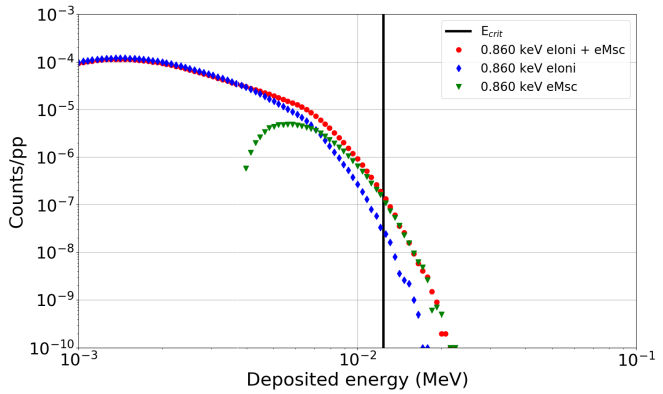

Fig. 15. Contribution to the energy deposition of 10 MeV protons of electron ionization and of electron multiple scattering events from the high-energy δ-rays.

very rare. Typically, the events leading to upset are driven by the combination of the energy deposition of 2–5 of these high-energy δ-rays depositing 1–10 keV.

The most noteworthy feature of these δ-rays is that they tend to deposit their whole energy inside the SV. Considering the continuous slow down approximation (CSDA) range of δ-rays of these energies and the characteristic sizes of the SV (thickness = 250 nm and main diagonal = 939 nm), the maximum energies that a δ-ray would be capable of depositing is $\sim$2.5 and $\sim$5.5 keV, respectively.

Fig. 14 depicts the fraction of kinetic energy that the δ-rays actually deposit in the SV as a function of their kinetic energy. The figure only considers the δ-rays that can contribute to the generation of an upset event. It is evident that most of these δ-rays actually deposit their full energy in the SV, even if their kinetic energy exceed, even by five times and by two times (up to 13 keV) the values obtained from the CSDA for the thickness and the main diagonal, respectively. Ultimately, it is because these δ-rays can deposit such large amounts of energy that such a large number of upsets from proton direct ionization are observed.

The reason behind these large energy depositions from δ-rays is related to the fact that δ-rays undergo strong scattering within the medium rather than moving through straight lines. Coulomb scattering events make the trajectory of these δ-rays inside the SV much longer than the characteristic sizes of the SV (either thickness or diagonal), allowing them to deposit their full kinetic energy.

The importance of Coulomb scattering events is evident in Fig. 13, where it is shown that, if these events are excluded, there is a huge decrease in the amount of δ-rays that can contribute to upsetting the SRAM.

As shown in Fig. 15, if Coulomb scattering events of δ-rays are disabled, a strong reduction of the total energy deposition spectra above the critical energy would occur. As a result, 84% of the events leading to an upset would not be correctly reproduced. Therefore, δ-ray Coulomb scattering events yield a six-fold increase in the number of upsets with respect to the sole electron ionization.

In conclusion, what is shown through this detailed scoring analysis is that it would not be correct to consider that all δ-rays produced above a certain energy ($\sim$5 keV) deposit their full kinetic energy in the SV. At the same time, a fraction of these δ-rays will still deposit their full kinetic energy in the SV, due to Coulomb scattering events, resulting in the observed proton direct ionization events at tens of MeV.

Concerning the potential impact of these δ-ray-induced upsets on the upset rate for space applications, this was covered in a previous study [16], where the upset rates of the RADSAGA and ISSI SRAMs were calculated with various methods. The results of that analysis pointed out that the LEP response dominates the upset rate over the intemediate- and high-energy responses for both SRAMs. Therefore, no specific implications on the upset rate related to the observations of proton direct ionization upsets at tens of MeVs would have to be drawn.

VI. Conclusion

The article reports about proton direct ionization phenomena impacting the SEU cross section of a highly integrated SRAM with low core voltage. The main focus is on the observation of an enhanced proton SEU cross section at tens of MeVs, which can be attributed, through comparison with neutron experiments and detailed scoring MC simulations, to proton direct ionization.

SV models and MC simulations showed that it was possible to reconstruct the experimental response of the SRAM as a function of primary proton energy under monoenergetic proton beams. The numerical tools provided by G4SEE were used to separate the various physical processes contributing to the triggering of SEUs in this SRAM, and in a second one for comparison purposes only. Direct ionization from protons was shown to be the process presenting the largest differences among the two SRAMs. For the chip under study, direct ionization is expected to be the dominant contributor at 10 MeV, a significant contributor at 20 MeV and as important as the nuclear elastic scattering at higher energies.

The detailed scoring of the MC simulations showed that high-energy (>0.860 keV) δ-rays generated inside and outside the SV are determinant in the triggering of upsets at primary proton energies above 3 MeV. A small amount of these high-energy δ-rays (2–5) produced by a single proton can deposit enough energy to exceed the critical energy of the SRAM.

Although having a range longer than the characteristic sizes of the SV according to the CSDA, these δ-rays can deposit their full kinetic energy in the SV even when being generated with a kinetic energy of 13 keV. This is due to Coulomb scattering events, that significantly increase the actual path of the δ-ray inside the SV and that result in a six-fold increment of the number of events exceeding the critical energy of the SRAM with respect to the sole electron ionization process.

Concerning MC simulations, this work shows, on the one hand, how important it is to set low-enough production thresholds for δ-rays in order to avoid overestimations in the SEU cross sections and, on the other hand, that the accurate transport of these high-energy δ-rays is fundamental in the understanding of the experimentally observed SEU cross sections, because the latter may be not fully related to well-known concepts, such as the proton LET and the CSDA.

Acknowledgment

The authors would like to thank Yolanda Morilla and Pedro Martìn-Holgado from CNA; Heikki Kettunen, Mikko Rossi,

and Jukka Jaatinen from RADEF; Marc-Jan van Goethem, Harry Kiewiet, Emil van der Graaff, and Sytze Brandenburg from Kernfysisch Versneller Instituut - Center for Advanced Radiation Technology (KVI-CART); Wojtek Hajdas, Laura Sinkunaite, and Miroslaw Marszalek from PSI; and Salvatore Fiore from FNG for their support during data collection at the respective facilities.

REFERENCES

[1] K. P. Rodbell, D. F. Heidel, H. H. K. Tang, M. S. Gordon, P. Oldiges, and C. E. Murray, "Low-energy proton-induced single-event-upsets in 65 nm node, silicon-on-insulator, latches and memory cells," *IEEE Trans. Nucl. Sci.*, vol. 54, no. 6, pp. 2474–2479, Dec. 2007.

[2] L. D. Edmonds and K. J. Edmonds, "A method for estimating SEU rates from protons by direct ionization," *IEEE Trans. Nucl. Sci.*, vol. 55, no. 5, pp. 2666–2678, Oct. 2008.

[3] D. F. Heidel *et al.*, "Low energy proton single-event-upset test results on 65 nm SOI SRAM," *IEEE Trans. Nucl. Sci.*, vol. 55, no. 6, pp. 3394–3400, Dec. 2008.

[4] R. K. Lawrence, J. F. Ross, N. F. Haddad, R. A. Reed, and D. R. Albrecht, "Soft error sensitivities in 90 nm bulk CMOS SRAMs," in *Proc. IEEE Radiat. Effects Data Workshop*, Quebec City, QC, Canada, Jul. 2009, pp. 123–126.

[5] B. D. Sierawski *et al.*, "Impact of low-energy proton induced upsets on test methods and rate predictions," *IEEE Trans. Nucl. Sci.*, vol. 56, no. 6, pp. 3085–3092, Dec. 2009.

[6] J. A. Pellish *et al.*, "Impact of spacecraft shielding on direct ionization soft error rates for sub-130 nm technologies," *IEEE Trans. Nucl. Sci.*, vol. 57, no. 6, pp. 3183–3189, Dec. 2010.

[7] C. Weulersee, F. Miller, D. Alexandrescu, E. Schaefer, and R. Gaillard, "Assessment and comparison of the low-energy proton sensitivity in 65 nm to 28 nm SRAM devices," in *Proc. RADECS Conf.*, Seville, Spain, Sep. 2011, pp. 291–296.

[8] N. Seifert, B. Gill, J. A. Pellish, P. W. Marshall, and K. A. LaBel, "The susceptibility of 45 and 32 nm bulk CMOS latches to low-energy protons," *IEEE Trans. Nucl. Sci.*, vol. 58, no. 6, pp. 2711–2718, Dec. 2011.

[9] J. R. Schwank *et al.*, "Hardness assurance testing for proton direct ionization effects," *IEEE Trans. Nucl. Sci.*, vol. 59, no. 4, pp. 1197–1202, Aug. 2012.

[10] J. A. Pellish *et al.*, "Criticality of low-energy protons in single-event effects testing of highly-scaled technologies," *IEEE Trans. Nucl. Sci.*, vol. 61, no. 6, pp. 2896–2903, Dec. 2014.

[11] N. A. Dodds *et al.*, "Hardness assurance for proton direct ionization-induced SEEs using a high-energy proton beam," *IEEE Trans. Nucl. Sci.*, vol. 61, no. 6, pp. 2904–2914, Dec. 2014.

[12] N. A. Dodds *et al.*, "The contribution of low-energy protons to the total on-orbit SEU rate," *IEEE Trans. Nucl. Sci.*, vol. 62, no. 6, pp. 2440–2451, Dec. 2015.

[13] N. A. Dodds *et al.*, "New insights gained on mechanisms of low-energy proton-induced SEUs by minimizing energy straggle," *IEEE Trans. Nucl. Sci.*, vol. 62, no. 6, pp. 2822–2829, Dec. 2015.

[14] J. Guillermin, N. Sukhaseum, P. Pourrouquet, N. Chatry, F. Bezerra, and R. Ecoffet, "Worst-case proton contribution to the direct ionization SEU rate," in *Proc. RADECS Conf.*, Geneva, Switzerland, Sep. 2017, pp. 330–337.

[15] B. Ye *et al.*, "Low energy proton induced single event upset in 65 nm DDR and QDR commercial SRAMs," *Nucl. Instrum. Methods Phys. Res. Sect. B, Beam Interact. Mater. At.*, vol. 406, pp. 443–448, Sep. 2017.

[16] A. Coronetti *et al.*, "Assessment of proton direct ionization for the radiation hardness assurance of deep sub-micron SRAMs used in space applications," *IEEE Trans. Nucl. Sci.*, vol. 68, no. 5, pp. 937–948, May 2021.

[17] PSTAR. *National Institute of Standards and Technology*. Accessed: May 2020. [Online]. Available: https://physics.nist.gov/PhysRefData/Star/Text/PSTAR.html

[18] J. F. Ziegler and J. P. Biersack. *Stopping and Range of Ions in Matter*. Accessed: Aug. 2018. [Online]. Available: http://www.srim.org

[19] A. Akkerman, J. Barak, and N. M. Yitzhak, "Role of elastic scattering of protons, muons, and electrons in inducing single-event upsets," *IEEE Trans. Nucl. Sci.*, vol. 64, no. 10, pp. 2648–2660, Aug. 2017.

[20] P. Caron, C. Inguimbert, L. Artola, R. Ecoffet, and F. Bezerra, "Physical mechanisms of proton-induced single-event upset in integrated memory devices," *IEEE Trans. Nucl. Sci.*, vol. 66, no. 7, pp. 1404–1409, Jul. 2019.

[21] Z. Wu, S. Chen, J. Yu, J. Chen, P. Huang, and R. Song, "Recoil-ion-induced single event uspets in nanometer CMOS SRAM under low-energy proton radiation," *IEEE Trans. Nucl. Sci.*, vol. 64, no. 1, pp. 654–664, Jan. 2017.

[22] M. P. King *et al.*, "Electron-induced single event upsets in static random access memories," *IEEE Trans. Nucl. Sci.*, vol. 60, no. 6, pp. 4122–4129, Dec. 2013.

[23] M. J. Gadlage, A. H. Roach, A. R. Duncan, M. W. Savage, and M. J. Kay, "Electron-induced single-event upsets in 45-nm and 28-nm bulk CMOS SRAM-based FPGAs operating at nominal voltage," *IEEE Trans. Nucl. Sci.*, vol. 62, no. 6, pp. 2717–2724, Dec. 2015.

[24] M. P. King *et al.*, "The impact of delta-rays on single-event upsets in highly scaled SOI SRAMs," *IEEE Trans. Nucl. Sci.*, vol. 57, no. 6, pp. 3169–3175, Dec. 2010.

[25] W. J. Stapor and P. T. McDonald, "Practical approach to ion track energy distribution," *J. Appl. Phys.*, vol. 64, p. 4430, Aug. 1988.

[26] A. Akkerman and J. Barak, "Ion-track structure and its effects in small size volumes of silicon," *IEEE Trans. Nucl. Sci.*, vol. 49, no. 6, pp. 3022–3031, Dec. 2002.

[27] Y. Morilla *et al.*, "Progress of CNA to become the Spanish facility for combined irradiation testing in aerospace," in *Proc. 18th Eur. Conf. Radiat. Effects Compon. Syst. (RADECS)*, Gothenburg, Sweden, Sep. 2018, pp. 250–254.

[28] A. Virtanen, R. Harboe-Sorensen, A. Javanainen, H. Kettunen, H. Koivisto, and I. Riihimaki, "Upgrades for the RADEF facility," in *Proc. IEEE Radiat. Effects Data Workshop*, Honolulu, HI, USA, Jul. 2007, pp. 38–41.

[29] H. Kettunen *et al.*, "Low energy protons at RADEF—Application to advanced eSRAMs," in *Proc. IEEE Radiat. Effects Data Workshop (REDW)*, Paris, France, Jul. 2014, pp. 147–150.

[30] E. R. van der Graaf, R. W. Ostendorf, M. J. van Goethem, H. H. Kiewiet, M. A. Hofstee, and S. Brandenburg, "AGORFIRM, the AGOR facility for irradiations of material," in *Proc. Eur. Conf. Radiat. Effects Compon. Syst.*, Bruges, Belgium, Sep. 2009, pp. 451–454.

[31] W. Hajdas, F. Burri, C. Eggel, R. Harboe-Sorensen, and R. de Marino, "Radiation effects testing facilities in PSI during implementation of the proscan project," in *Proc. IEEE Radiat. Effects Data Workshop*, Phoenix, AZ, USA, Jul. 2002, pp. 160–164.

[32] A. Coronetti *et al.*, "SEU characterization of commercial and custom-designed SRAMs based on 90-nm technology and below," in *Proc. IEEE Radiat. Effects Data Workshop*, Santa Fe, NM, USA, Dec. 2020, pp. 56–63.

[33] M. Cecchetto *et al.*, "0.1–10 MeV neutron soft error rate in accelerator and atmospheric environments," *IEEE Trans. Nucl. Sci.*, vol. 68, no. 5, pp. 873–883, May 2021.

[34] A. Pietropaolo *et al.*, "The Frascati neutron generator: A multipurpose facility for physics and engineering," *J. Phys., Conf.*, vol. 1021, May 2018, Art. no. 012004, doi: 10.1088/1742-6596/1021/1/012004.

[35] J. Wang, J. Prinzie, A. Coronetti, and P. Leroux, "Study of the SEU sensitivity of an SRAM-based radiation monitor in a 65-nm CMOS technology," *IEEE Trans. Nucl. Sci.*, vol. 68, no. 5, pp. 913–920, May 2021.

[36] J. Allison *et al.*, "Geant4 developments and applications," *IEEE Trans. Nucl. Sci.*, vol. 53, no. 1, pp. 270–278, Feb. 2006.

[37] D. Lucsányi, R. García Alía, K. Bilko, M. Cecchetto, S. Fiore, and E. Pirovano, "G4SEE: A geant4-based single event effect simulation toolkit and its validation through monoenergetic neutron measurements," *IEEE Trans. Nucl. Sci.*, vol. 69, no. 3, pp. 273–281, Mar. 2022.

[38] G. Battistoni *et al.*, "Overview of the FLUKA code," *Ann. Nucl. Energy*, vol. 82, pp. 10–18, Aug. 2015.

[39] T. T. Böhlen *et al.*, "The FLUKA code: Developments and challenges for high energy and medical applications," *Nucl. Data Sheets*, vol. 120, pp. 211–214, Jun. 2014.

[40] W. M. Yao *et al.*, "Review of Particle Physics," *J. Phys. G, Nucl. Part. Phys.*, vol. 33, no. 1, pp. 1–1232, Jul. 2006.